



RESEARCH ARTICLE

10.1002/2014GC005284

Key Points:

- Basalt-hosted inactive hydrothermal site Krasnov exhibits a magnetization low
- The magnetic signature of such sites survives the end of hydrothermal activity
- Presence of sulfides and alteration of magnetized basalt are the major causes

Correspondence to:

J. Dymant,
jdy@ipgp.fr

Citation:

Szitkar, F., J. Dymant, Y. Choi, and Y. Fouquet (2014), What causes low magnetization at basalt-hosted hydrothermal sites? Insights from inactive site Krasnov (MAR 16°38'N), *Geochem. Geophys. Geosyst.*, 15, doi:10.1002/2014GC005284.

Received 11 FEB 2014

Accepted 31 MAR 2014

Accepted article online 2 APR 2014

What causes low magnetization at basalt-hosted hydrothermal sites? Insights from inactive site Krasnov (MAR 16°38'N)

Florent Szitkar¹, Jérôme Dymant¹, Yujin Choi¹, and Yves Fouquet²

¹Institut de Physique du Globe de Paris, CNRS, Sorbonne Paris Cité, Université Paris Diderot, Paris, France, ²IFREMER Centre de Brest, Plouzané, France

Abstract High-resolution magnetic surveys acquired near the seafloor show that active basalt-hosted hydrothermal sites are associated with zones of lower magnetization. This observation may reflect the thermal demagnetization of a hot hydrothermal zone, the alteration of basalt affected by hydrothermal circulation, and/or the presence of thick, nonmagnetic hydrothermal deposits. In order to discriminate among these inferences, we acquired vector magnetic data 50 m above inactive hydrothermal site Krasnov using the Remotely Operated Vehicle (ROV) *Victor*. This deep hydrothermal site, located 7 km east of the Mid-Atlantic Ridge (MAR) axis at 16°38'N, is dissected by major normal faults and shows no evidence of recent hydrothermal activity. It is therefore a perfect target for investigating the magnetic signature of an inactive basalt-hosted hydrothermal site. Krasnov exhibits a strong negative magnetic anomaly, which implies that the lower magnetization observed at basalt-hosted hydrothermal sites is not a transient effect associated with hydrothermal activity, but remains after activity ceases. Thermal demagnetization plays only a secondary role, if any, in the observed magnetic low. Forward models suggest that both the nonmagnetic hydrothermal deposits and an altered zone of demagnetized basalt are required to account for the observed magnetic low. The permanence of this magnetic signature makes it a useful tool to explore midocean ridges and detect inactive hydrothermal sites.

1. Introduction

Active basalt-hosted hydrothermal sites exhibit a magnetic low, i.e., a negative reduced-to-the-pole (RTP) magnetic anomaly or a low equivalent magnetization, as observed on the TAG (Trans-Atlantic Geotraverse) hydrothermal site, Mid-Atlantic Ridge (MAR) 26°08'N [Tivey *et al.*, 1993], the Endeavour segment, Juan de Fuca Ridge [Johnson *et al.*, 2002; Tivey and Johnson, 2002], several sites on the Central MAR and on the southern MAR at 4°48'S [Tivey and Dymant, 2010], the Southwest Indian Ridge at 49°39'E [Zhu *et al.*, 2010], the Brothers Seamount in the Havre Trough [Caratori-Tontini *et al.*, 2012a], the southern Mariana Trough [Nakamura *et al.*, 2013], and the Izu-Ogasawara Arc [Honsho *et al.*, 2013]. Most of these results have been obtained from near-seafloor magnetic measurements, because the limited areal extent of hydrothermal sites—generally of the order of several hundred meters—is not resolvable at the sea surface, 1.5–4 km away.

Three processes may explain these observations:

1. The temperature measured at active hydrothermal sites reaches several hundred degrees, exceeding the Curie temperature of titanomagnetite—the primary magnetic mineral in midocean ridge extrusive basalt—which ranges between 150 and 200°C [e.g., Kent and Gee, 1996]. Thermal demagnetization of basalt may therefore explain the magnetic lows at basalt-hosted hydrothermal sites [e.g., Tivey *et al.*, 1993, 1996]. This effect is transient and the basalt recovers its magnetization after cessation of hydrothermal activity.

2. The pervasive circulation of hot hydrothermal fluids beneath hydrothermal sites results in the alteration of titanomagnetite to less magnetic titanomaghemite [Ade-Hall *et al.*, 1971; Johnson and Pariso, 1987; Watkins and Paster, 1971] and ultimately to nonmagnetic minerals, resulting in lower magnetization [e.g., Tivey and Johnson, 2002]. This process involves permanent chemical and mineralogical transformations: the altered material remains demagnetized after cessation of hydrothermal activity.

3. The presence of a thick, nonmagnetic or weakly magnetized hydrothermal deposit increases the distance between the magnetic measurements and any underlying magnetized lavas, resulting in an apparent magnetic low.

Most previous studies have focused on active hydrothermal sites and do not address the relative importance of these different processes in generating the observed magnetic lows. Only Tivey and Johnson [2002] surveyed

basalt-hosted hydrothermal sites at different stages of their evolution on the Endeavour segment, Juan de Fuca Ridge, including some inactive sites. They found that these inactive sites are also associated with a weak magnetization and concluded that alteration is the primary process causing this weak magnetization. These inactive sites, however, lie <500 m away from active sites and may still be associated with a thermal anomaly. We readdress the question of how the magnetic signature of basalt-hosted sites evolves after the end of hydrothermal activity by investigating a fully extinct hydrothermal site. To do so, we surveyed the inactive basalt-hosted hydrothermal site Krasnov during cruise Serpentine in 2007 [Fouquet *et al.*, 2008] and collected high-resolution bathymetric and magnetic data. We demonstrate that a strong magnetic low is present over Krasnov, suggesting that both the presence of nonmagnetic hydrothermal deposits and magnetic mineral alteration are the dominant effects explaining the observed magnetic signature at basalt-hosted hydrothermal sites.

Specific geological contexts, such as the presence of abundant sediments or the occurrence of magma-poor seafloor spreading, result in different processes and therefore different magnetic signatures (e.g., Tivey [1994] and Gee *et al.* [2001] for the sediment-hosted sites of Middle Valley, Juan de Fuca Ridge; Dymant *et al.* [2005], Tivey and Dymant, [2010], and F. Sztikar *et al.* (Deep-Sea magnetism unveils mineral-rich ultramafic-hosted hydrothermal sites, submitted to *Geology*, 2014), for the ultramafic-hosted sites of the MAR). These specific contexts are not considered in this study.

2. Geological Setting

Krasnov is located on the Mid-Atlantic Ridge, at 16°38'30"N 46°29'W, 7 km east of the spreading axis marked by an axial volcanic ridge (Figure 1) [Bel'tenev *et al.*, 2004]. Discovered in 2002, it is one of the largest and deepest known hydrothermal fields (3600–3800 m). The site is located near the crest of the eastern axial valley wall, immediately south of a large oblique volcanic structure that extends into the axial valley (Figure 1). The site is at the intersection of two major normal faults: one trending N20°E, parallel to the axial valley wall, and the other one N135°E, along the oblique volcanic structure (Figure 2a) [Cherkashov *et al.*, 2008; Fouquet *et al.*, 2008]. Numerous landslides have generated debris talus covering the lower part of these fault scarps [Cannat *et al.*, 2013]. The thickness of these talus deposits increases westward, as the bathymetry deepens.

The areal extent of Krasnov hydrothermal site is based on data from Cherkashov *et al.* [2008] modified using our Cruise Serpentine high-resolution bathymetry and dive observations. Two hydrothermal mounds are observed as part of an 800 × 900 m wide zone covered by metalliferous sediments [Cherkashov *et al.*, 2008]. A small sulfide mound, 100 × 100 m wide, is located to the north while a larger mound, 300 × 500 m wide, is located to the south. The latter is cut by the previously mentioned major faults near their intersection and results in a residual half mound feature with a steep N-S trending, west-facing 70–100 m high fault scarp exposing massive sulfides [Cherkashov *et al.*, 2008]. A horseshoe-shaped landslide structure below reflects a mechanically weaker zone in the hydrothermal area (Figure 2a). Further downslope, at ~3740 m lies a large, 150 × 100 m tilted landslide block with outcropping sulfide deposits. This block is cut by a second-order, 10 m scarp [Cannat *et al.*, 2013]. The southern boundary of the hydrothermal area is poorly defined, as it corresponds to a steep debris corridor. The sulfide deposits have been dated 5.6–119.2 ka by the U/Th method [Cherkashov *et al.*, 2008], younger than the last magnetic polarity reversal (Brunhes-Matuyama, 780 ka according to the geomagnetic polarity time scale of Cande and Kent [1995]).

3. Magnetic Survey and Results

During cruise Serpentine of R/V *Pourquoi pas?* in 2007, we collected high-resolution bathymetric and magnetic data using ROV *Victor* of Ifremer. Bathymetric data were acquired by a RESON SeaBat 7125 multibeam echosounder [Cannat *et al.*, 2013] and the magnetic data by a three-component fluxgate magnetometer. The ROV surveyed east-west parallel profiles, spaced 120 m apart and 50 m (± 5 m) above the seafloor over an area of ~3000 × 1500 m. No crossing line was performed. The bathymetric grid, presented by Cannat *et al.* [2013], has a resolution of 0.5 m and extends across the axial valley wall from depth ~3600 to ~4400 m (Figure 2a).

The ROV magnetic susceptibility tensor A (nine coefficients) and remanent magnetization vector H_p (three coefficients) were estimated using the method developed by Isezaki [1986], and Honsho *et al.* [2009], based on "calibration loops" performed during the descent and ascent of the ROV, at distance from both the ship and the seafloor. Assuming a damping factor of 7 [Honsho *et al.*, 2009], we obtain

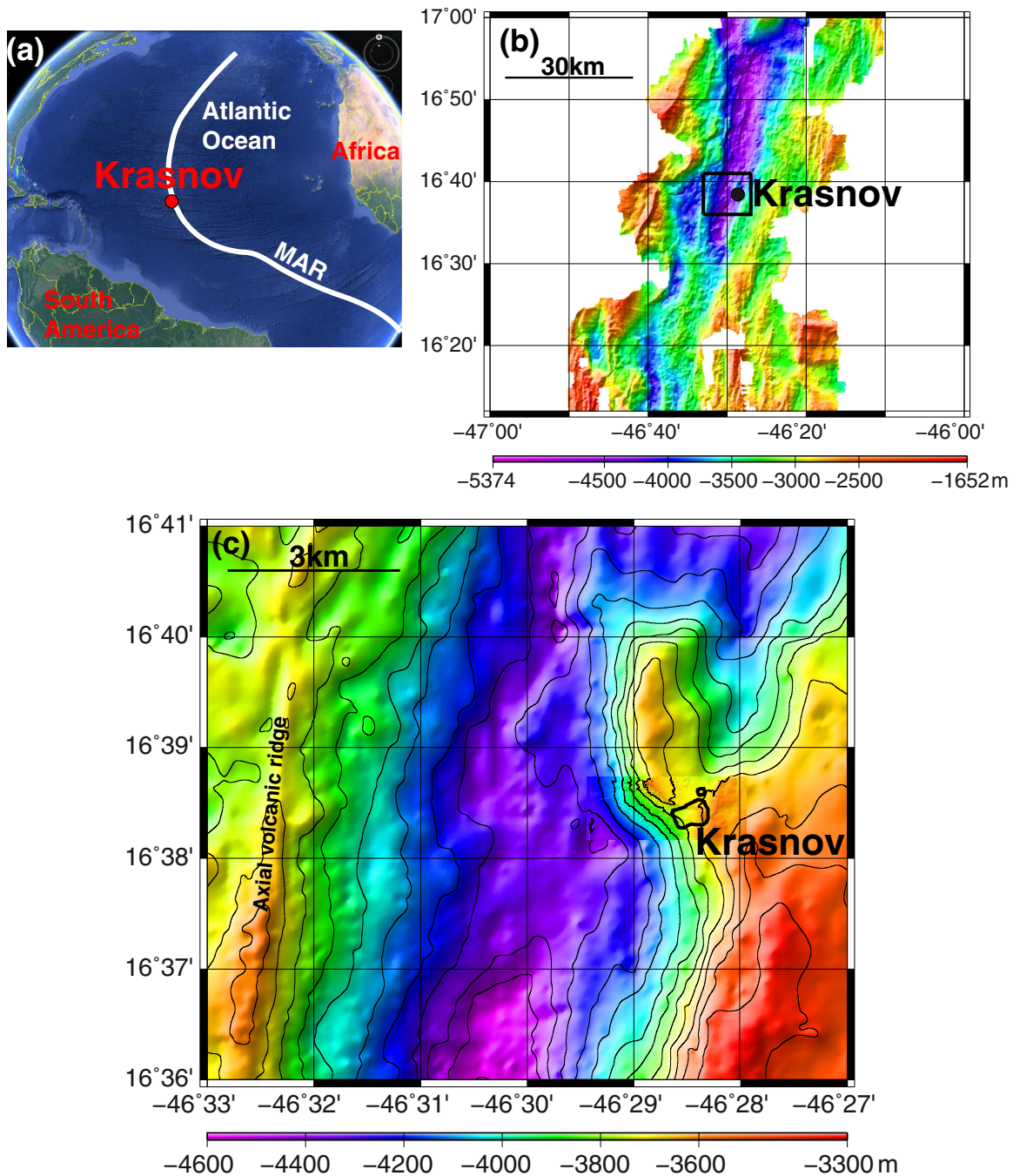


Figure 1. (a) Localization of site Krasnov along the Mid-Atlantic Ridge. (b) Ship-borne multibeam bathymetry of the Mid-Atlantic Ridge between 16°12' and 17°N, in site Krasnov area. The black box delineates the enlargement of Figure 1c. (c) Enlargement showing the tectonic setting of hydrothermal site Krasnov, with the high-resolution bathymetry collected by ROV Victor superimposed. Black contours delineate the inactive hydrothermal area.

$$A = \begin{pmatrix} 0.0248 & 0.0260 & 0.0008 \\ -0.0228 & 0.0207 & -0.0041 \\ -0.0716 & -0.0501 & 0.0259 \end{pmatrix} \text{ and } H_p = \begin{pmatrix} 2646 \\ -249 \\ 1575 \end{pmatrix}$$

which are used to remove the magnetic effect of the submersible from the vector magnetic measurements. The resulting vector magnetic field is converted to geographical coordinates and transformed to vector magnetic anomaly by removing the geomagnetic field, approximated by the IGRF [IAGA Working Group

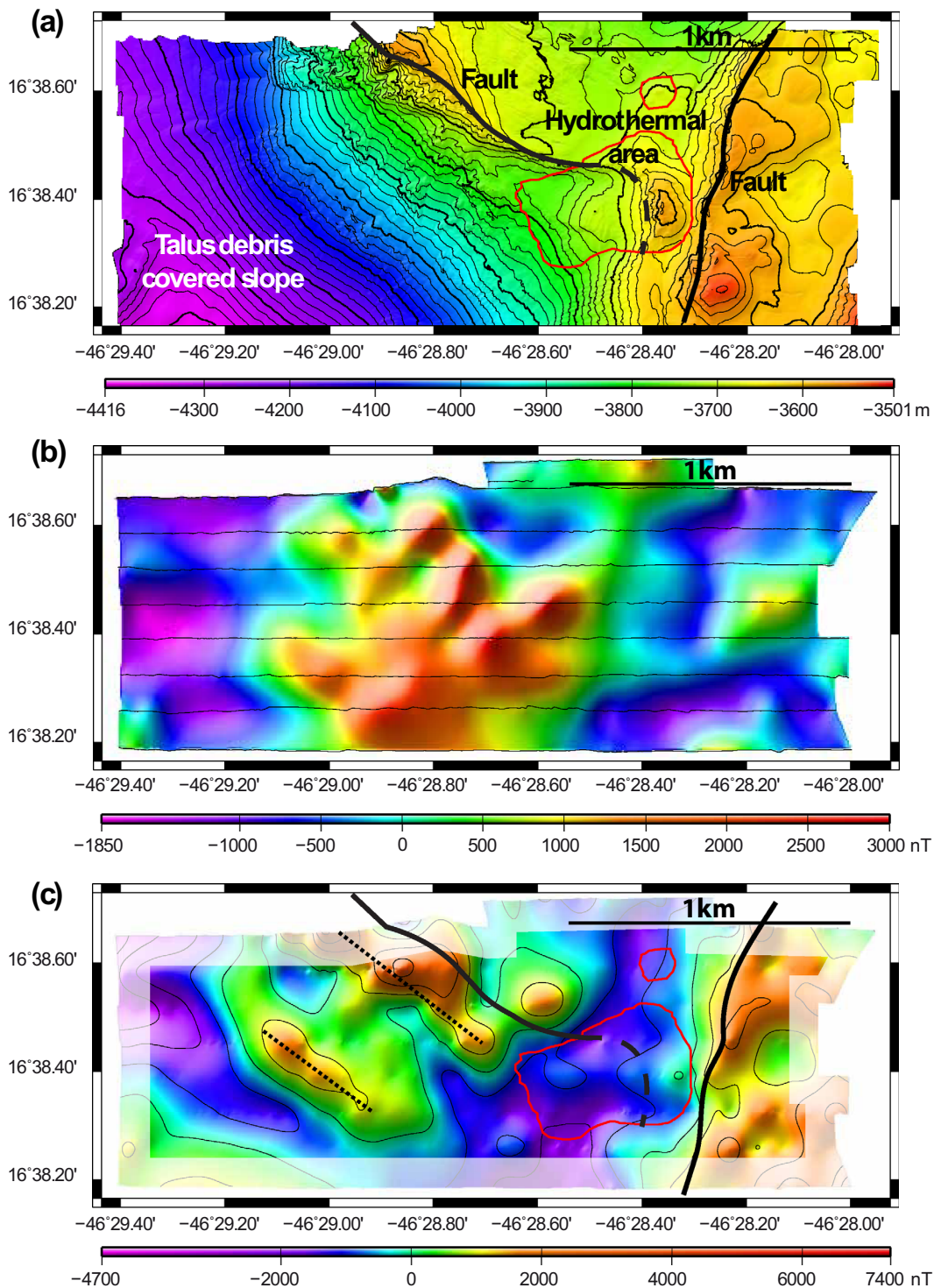


Figure 2. High-resolution data collected by ROV Victor, 50 m above seafloor in site Krasnov area. (a) Multibeam bathymetry. (b) Magnetic anomaly. Black lines correspond to the submersible tracks. (c) Reduced-to-the-pole (RTP) magnetic anomaly. Red contours delineate the inactive hydrothermal area, black lines the major faults. Dotted lines correspond to the two parallel magnetic features discussed in text. The pale stripe on the map edges delineates the area which may have been affected by the extrapolation required to achieve the ABIC inversion (see text for details); less confidence should be given to the RTP anomaly in this area. The inactive hydrothermal site is associated with a strong negative RTP anomaly.

V-MOD, 2010]. Practically, the corrections correspond to a total remanent field of 3089 nT and a total induced field of at most 2443 nT, depending orientation, for ROV Victor. These corrections compare to a range of 4850 nT for the resulting total field anomaly (Figure 2b). An independent way to check the

reliability of this processing scheme is the lack of any heading influence on the final map. The residual magnetic anomaly data along the submersible tracks were filtered to remove wavelengths shorter than 75 m, and interpolated onto a 5 m spaced grid by a nearest neighbor algorithm [Smith and Wessel, 1990]. Finally, the anomaly was reduced-to-the-pole (RTP). Such a transformation helps the interpretation by placing the anomalies above their causative sources, whereas the original anomalies are usually not due to the combined effect of nonvertical magnetization and ambient magnetic field vectors. It provides reliable results if the survey area is located $>10^\circ$ away from the magnetic equator. This operation is easily achieved by a simple filter applied in the Fourier domain for magnetic data acquired at a constant altitude [e.g., Baranov, 1957]. It is, however, nontrivial for magnetic data acquired on an uneven surface. To solve this issue, we inverted the magnetic anomalies to equivalent magnetization using the Akaike Bayesian Information Criterion (ABIC) method of Honsho *et al.* [2012, 2013], and recomputed magnetic anomalies at the pole (i.e., assuming vertical magnetization and ambient magnetic field vectors) under the same geometrical assumptions. The ABIC method takes full advantage of measurements acquired at varying altitudes above the seafloor, alleviating the need for upward continuation to a constant-elevation surface and the associated loss of resolution. The resulting RTP magnetic anomaly map is presented in Figure 2c.

The survey area is located within the axial magnetic anomaly and formed during the normal polarity Brunhes epoch, so a positive (respectively negative) RTP anomaly corresponds to a positive (respectively negative) magnetization contrast. The northern part of the surveyed area is dominated by a large positive anomaly associated with the faulted axial valley wall volcanic structure (Figure 2). This positive anomaly is split into two parallel magnetic features whose amplitudes decrease from 4500 to 1500 nT westward. The strongest, easternmost anomaly is located 120 m down the crest line separating the volcanic seafloor, to the northeast, and the N135°E fault scarp, to the southwest, at ~ 3500 – 3600 m. The second, weaker, magnetic feature is located further downslope. Both anomalies may reflect the top of tilted blocks, bearing a coherent magnetization, buried under talus debris made of randomly oriented and magnetically transparent, basaltic fragments. The strong magnetic anomaly lows observed on the southern and western ends of the survey area likely reflect the thick, magnetically transparent, debris talus accumulated at the foot of the slope, resulting in attenuated magnetic anomalies (Figure 2) [Cannat *et al.*, 2013].

The hydrothermal area (red lines, Figure 2c) corresponds to a marked negative magnetic anomaly, in agreement with the magnetic signature generally observed on basalt-hosted hydrothermal sites [e.g., Tivey and Dymert, 2010]. Both the larger southern hydrothermal mound and the smaller northern one exhibit a ~ 3500 nT magnetic low (crest to crest). The magnetic anomaly associated with the large mound affects both its undisturbed part, to the North and East, and tectonized part, to the South and West, suggesting that this anomaly cannot solely be the result of debris accumulation. However, the strongest negative anomaly is located at the southern end of the hydrothermal area, reflecting either a combined influence of the basalt-hosted hydrothermal site low magnetization and the nearby, magnetically transparent, debris corridor, or the presence of an eccentric, dipping hydrothermal pipe. This magnetic low may continue beyond the southern limit of Figure 2c.

4. Forward Modeling

The active faults which dissect the Krasnov hydrothermal deposit do not show evidence of more recent hydrothermal activity postdating the sulfide mound collapse. Such major faults are preferentially affected by fluid circulation. If the area was still associated with a significant thermal anomaly, these faults would certainly focus the associated hydrothermal activity. The lack of hydrothermal constructions postdating the fault activity, therefore, suggests that no significant thermal anomaly exists in the area anymore. Simple thermal calculations indicate that the cooling time of a thermal anomaly within the first 500 m of the oceanic crust is a few thousand years. If the hydrothermal activity ceased 5.6 kyr ago, as suggested by the youngest sulfide dated in the area [Cherkashov *et al.*, 2008], the associated thermal anomaly has almost completely disappeared and the temperature at 500 m depth is much lower than the Curie temperature of extrusive basalt titanomagnetite (150–200°C) [Kent and Gee, 1996]. The observed magnetic low is therefore unlikely to be the result of thermal demagnetization.

We investigate two other hypotheses to explain this magnetic signature: the presence of a nonmagnetic layer over the magnetic basement, and the presence of an altered hydrothermal pipe beneath the hydrothermal site.

We use forward modeling to constrain the characteristics of the nonmagnetic body. Due to the intrinsic nonuniqueness of the potential field solution, an infinite number of models can fit the observed anomalies. We make simplifying assumptions, i.e., magnetization invariant with depth within the magnetic layer and a vertical magnetization vector (consistent with the RTP magnetic anomaly), and restrict our modeling exercise to geographical variations of a limited number of parameters. Three parameters play a major role: the magnetization intensity, the magnetic layer thickness, and the thickness of the overlying nonmagnetic layer. The magnetization intensity is assumed to be constant at 12 A/m. This value is similar to those obtained on the nearby MAR at 21°40'N for, in one hand, the equivalent magnetization computed for a 500 m thick layer from sea-surface anomalies and, on the other hand, the absolute magnetization derived from deep-sea submersible observations [Honsho *et al.*, 2009]. The base of the magnetic layer is set at 500 m beneath the bathymetry. The shape of this interface is, however, of little significance, as the influence of a unit body at this interface is a thousand times weaker than the influence of the same body on the top of the magnetic layer. As a result, this bottom interface only produces a very weak, long wavelength component to the modeled anomalies. The only parameter varying in the following models is the thickness of the nonmagnetic layer overlying the magnetic basement. Synthetic anomalies are computed for the whole survey area, but only the results obtained for the hydrothermal site are presented on Figures 3 and 4. In order to avoid any edge effects and ensure a smooth transition at the border of these maps, we use the same hypotheses inside and outside the hydrothermal perimeter, i.e., 12 A/m, 500 m thick magnetized layer, and varying thicknesses of nonmagnetized layers, depending the model.

In order to optimize the computation time, the bathymetric grid is resampled at 2×2 m intervals (i.e., four times lower than the initial resolution of 0.5 m). Each node of this grid represents the center of a unit prism, which is assigned a magnetization (intensity and direction), a top and a base. For the sake of comparison with the real data, we compute the modeled anomaly at the locations of the measurement points, considering the effect of the prisms lying within a 1000×1000 m zone around these points. The computation at a given point therefore includes 250,000 contiguous prisms with no gap. Considering the average altitude of the ROV at 50 m above the seafloor, the distance between the computation point and the nearest prism not considered in the computation is ~ 503 m. The magnetic field strength decreasing as the cube of the distance, the relative influence of prisms at the center and the edge of the computation zone is more than a thousand. The influence of prisms located further away is neglected. Thanks to the width of the bathymetric swaths, the bathymetric grid extends beyond the magnetic measurement points, preventing any side effects for the areas presented in Figures 3 and 4.

4.1. Thickness of the Nonmagnetic Debris and Hydrothermal Deposits

We assume a 500 m thick layer of basalt bearing a 12 A/m magnetization, covered by a nonmagnetic layer with varying thickness. The nonmagnetic layer overlying the magnetic basement is a convenient way to model both the weakly magnetized hydrothermal deposits and the magnetically transparent mass-wasted material. Here we try to constrain its thickness in order to adjust the observed anomalies under the previously mentioned assumptions. In a first step, we assume that the nonmagnetic layer around the hydrothermal area, made of mass-wasted deposits, has a uniform thickness of 100 m. The nonmagnetic layer in the hydrothermal area, which combines both hydrothermal and debris material, is also assumed to be uniform. Forward models are computed for different values of this parameter ranging between 100 and 200 m. This range corresponds to a 100 m thick hydrothermal deposit, suggested by direct observation on the fault scarp [Cherkashov *et al.*, 2008; Fouquet *et al.*, 2008] and similar to the one drilled at the TAG hydrothermal mound [Humphris *et al.*, 1995], covered by 0–100 m thick mass-wasted material. Figure 3b presents the resulting anomalies for the maximum value of 100 m (nonmagnetic layer of 200 m in the hydrothermal area), which results in a magnetic anomaly too weak to explain the observations (Figure 3a). We doubt that this parameter can be reasonably increased. Conversely, the over-simplistic assumption of a constant thickness for the mass-wasted deposits around the hydrothermal area results in an inadequate modeling of second-order anomalies over these deposits. In a second step, we adjust the thickness of the nonmagnetic layer around the hydrothermal area to fit these second-order anomalies, again assuming a nonmagnetic layer of 100 m (Figure 3c) and 200 m (Figure 3d) in the hydrothermal area. The resulting thickness of the mass-wasted deposits ranges between 0 and 250 m and is consistent with a gradual southwestward thickening of these deposits. The magnetic anomaly predicted for a 100 m thick nonmagnetic layer is clearly inadequate (Figure 3c), and that for a 200 m thick nonmagnetic layer is slightly weaker (6000 nT crest-to-crest,

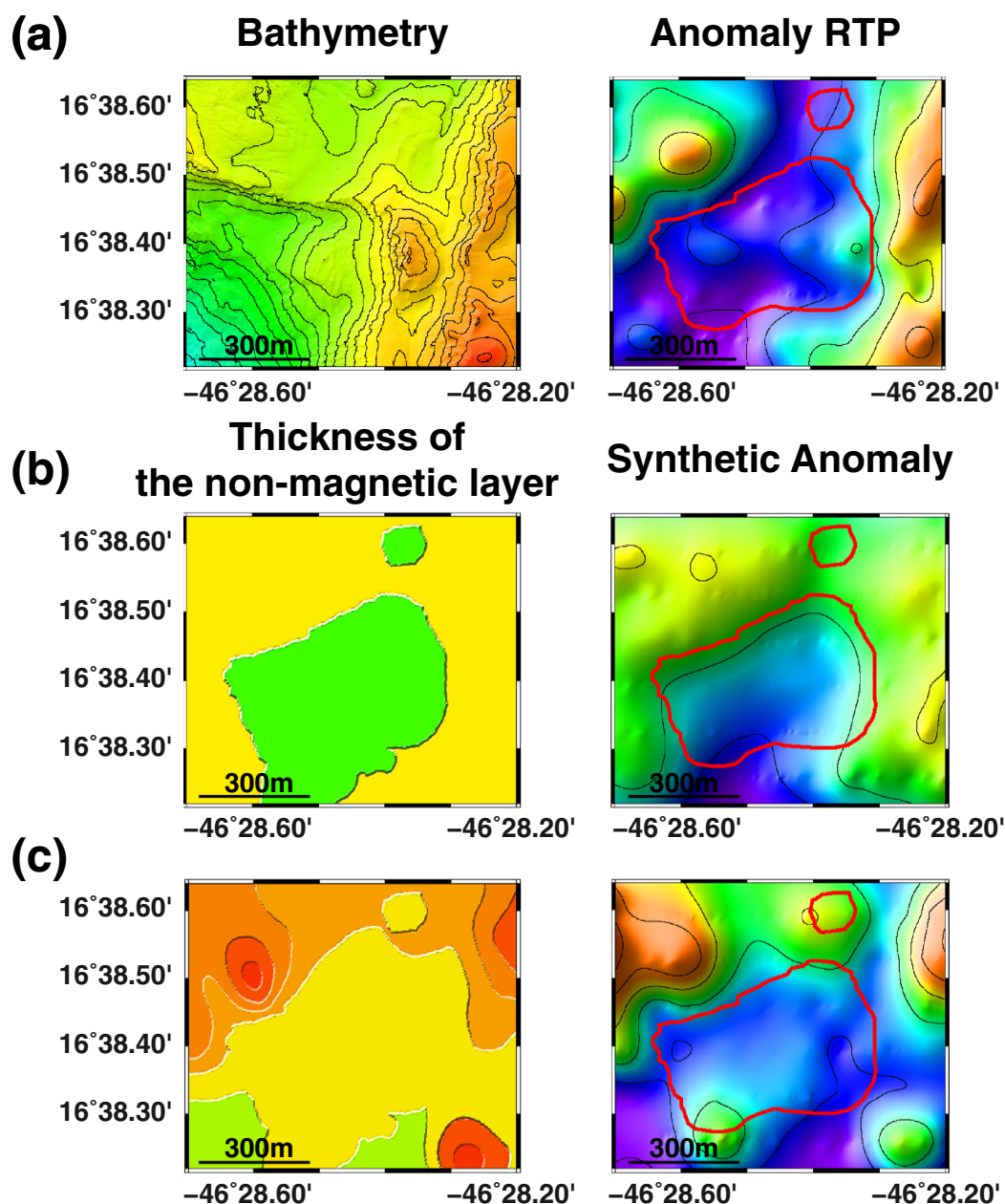


Figure 3. (a, left) High-resolution multibeam bathymetry and (right) reduced-to-the-pole magnetic anomaly in the Krasnov hydrothermal area. (b–f, left) Models assuming different thicknesses of the overlying nonmagnetic layer and (right) the corresponding magnetic anomaly. All models consider a vertical magnetization of constant intensity 12 A/m in a 500 m thick magnetic layer. The overlying nonmagnetic layer is 100 m thick around the hydrothermal area, where it is made of mass-wasted material, and 200 m thick in the hydrothermal area, where it is made of both debris and hydrothermal deposits (Figure 3b). The resulting anomaly associated with the hydrothermal area is much weaker than the observed one. The overlying nonmagnetic layer is adjusted in an ad hoc way around the hydrothermal area and is 100 m thick (Figure 3c) or 200 m thick (Figure 3d) in the hydrothermal area. The resulting anomaly in the hydrothermal area is still weaker than the observed one in Figure 3c and resembles the observed one, with misplaced second-order features, in Figure 3d. Idem, with the base of the nonmagnetic layer modeled by bicubic spline surfaces in the hydrothermal area (Figures 3e and 3f). This shape takes into account a superficial layer of mass-wasted and hydrothermal deposits and a deeper hydrothermal pipe of altered basalt. Both (e) narrower and (f) wider pipes result in anomalies resembling the observed one in the hydrothermal area.

Figure 3d) than the observed one (7200 nT, Figure 3a). Within these simple hypotheses, obtaining an acceptable synthetic anomaly can be achieved either by thickening the hydrothermal and/or mass-wasted deposit beyond 200 m, which seems geologically implausible, or by removing magnetization beneath the hydrothermal area, as it would be the case for altered, demagnetized basalt in an hydrothermal pipe.

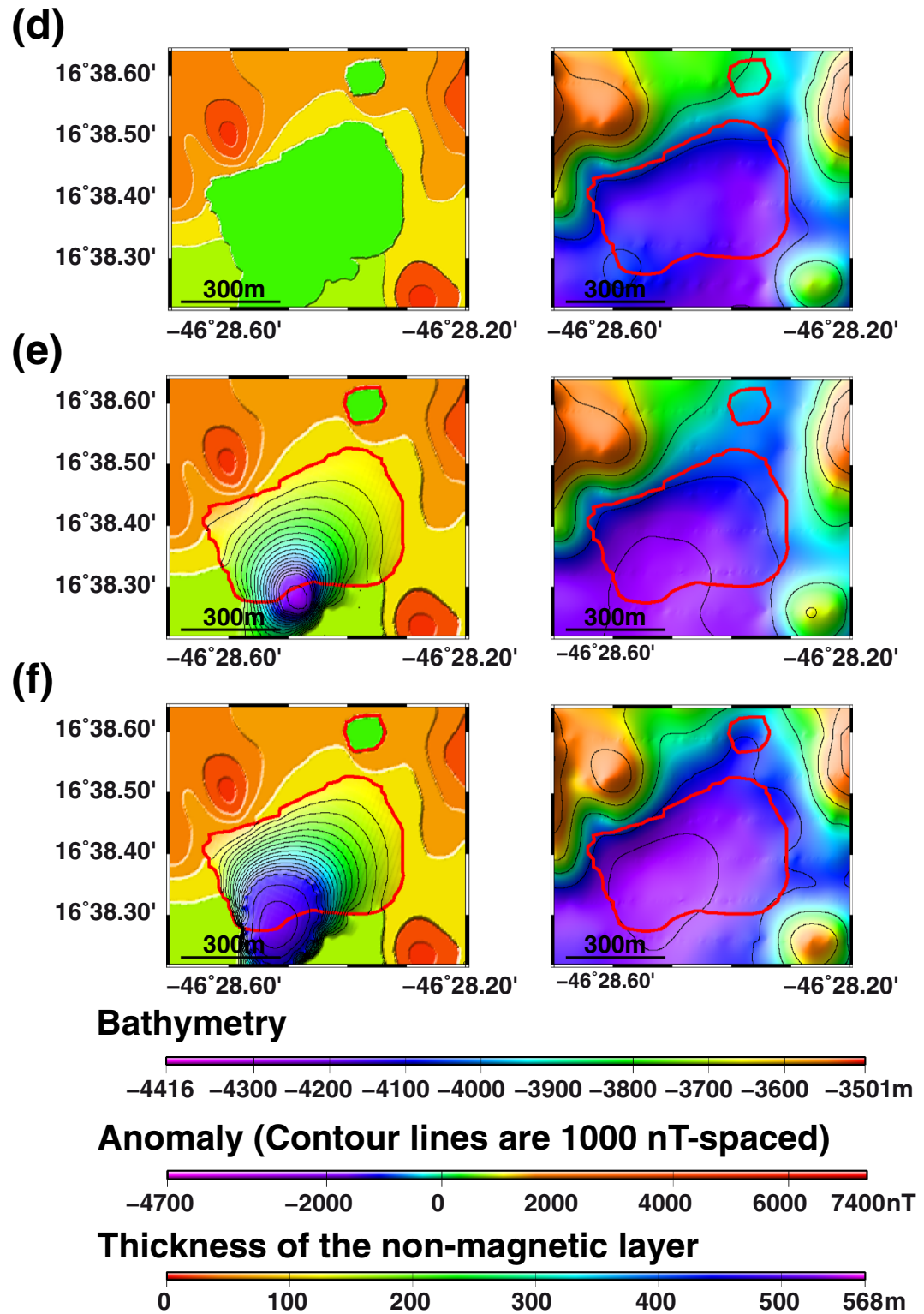


Figure 3. (Continued)

4.2. Shape of the Nonmagnetic Hydrothermally Altered Basalt

The previous model (Figure 3d) approaches the amplitude of the observed negative anomaly in the hydrothermal area, but fails to account for detailed variations such as the lowest anomaly located at its southern edge.

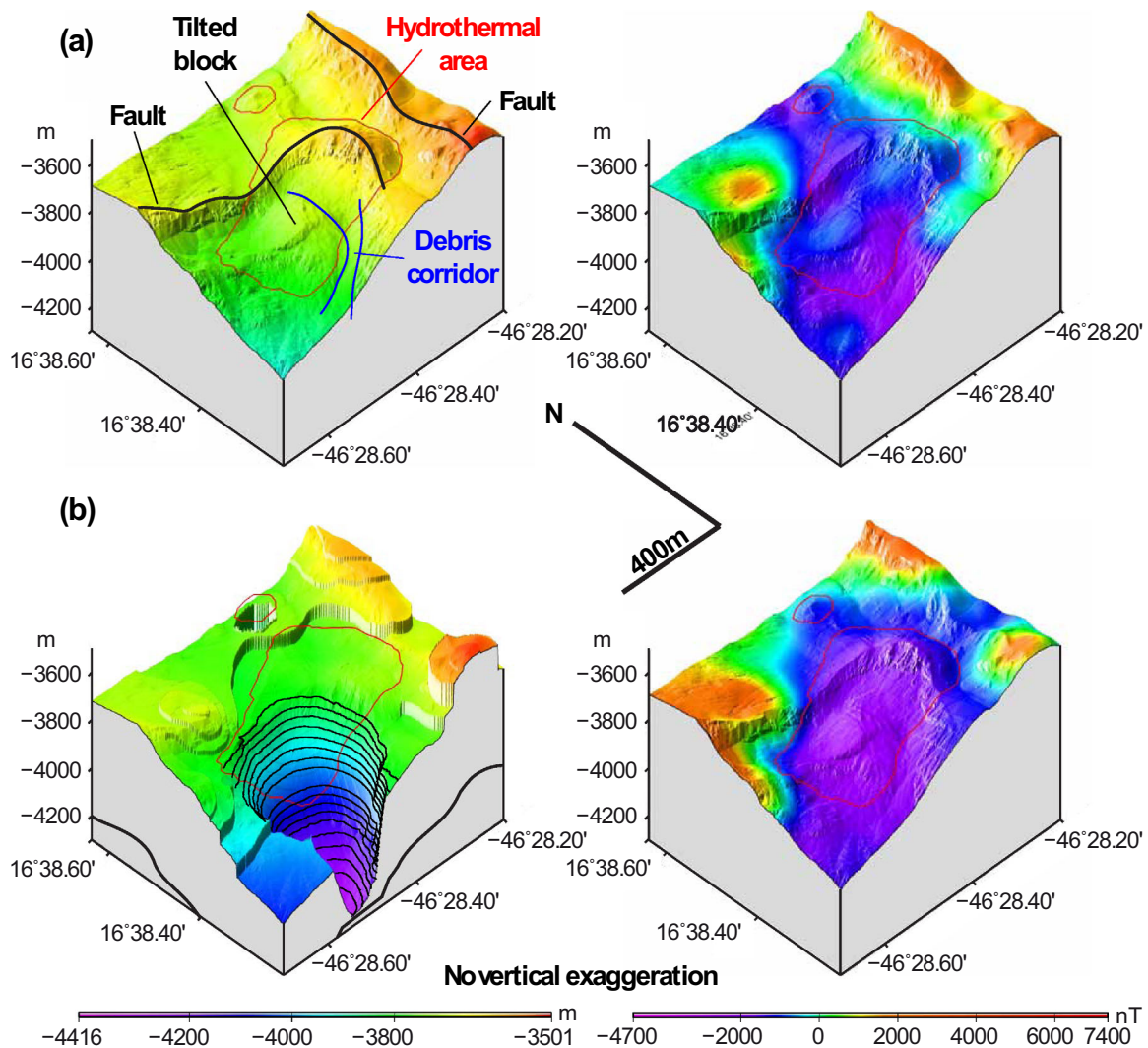


Figure 4. (a, left) Perspective view of the high-resolution multibeam bathymetry and (right) reduced-to-the-pole magnetic anomaly in the Krasnov hydrothermal area. (b) Perspective view of the base of the overlying nonmagnetic layer (left; thick lines on the block sides mark the base of the magnetic layer) and (right) the corresponding magnetic anomaly for the model presented in Figure 3f.

A possible explanation for such a discrepancy may be the presence of demagnetized basalt beneath the hydrothermal and/or mass-wasted deposits. In an attempt to constrain these demagnetized basalts, we consider a funnel-shaped surface encompassing the hydrothermal area and progressively deepening from edges (100–150 m deep for a smooth transition with surrounding areas) to center (570 m deep). The part of the 500 m thick basaltic layer located above this surface is altered and considered nonmagnetic, whereas that beneath this surface remains magnetized. In Figures 3e and 3f, we model this surface as a natural bicubic spline (i.e., a minimum curvature surface) [Smith and Wessel, 1990], the radius of the hydrothermal pipe at 350 m being fixed to 50 m (Figure 3e) and 125 m (Figure 3f) and its center located beneath the lowest RTP anomaly. The resulting computed anomalies compare well to the observed ones (Figure 3a), although it is difficult to discriminate between the two models due to the greater distance (>350 m) between the altered basalt and the observation points.

Neither models succeeded in predicting the slight relative magnetic high which cuts across the main hydrothermal area along an E-W direction on the observed RTP anomaly (Figures 3 and 4). This magnetic feature extends eastward the strong positive anomaly located ~120 m beneath the NW-SE fault scarp (Figure 2), which may mark the top of a coherent tilted block of magnetized basalt beneath debris or hydrothermal deposits (see above, section 3). Such an inference is supported by the association of the slight relative

magnetic high with the coherent tilted block observed in the hydrothermal area (see above, section 2) [Cannat *et al.*, 2013]. We made no attempt to model such variations of the magnetic basement, considering the lack of constraint on its geometry.

Our preferred model (Figure 4) considers two nonmagnetic layers: (1) a superficial, ~ 100 m thick layer covering the whole hydrothermal area, interpreted as mostly sulfide deposit based on the collected samples and direct observations [Cherkashov *et al.*, 2008; Fouquet *et al.*, 2008], and (2) a deeper zone, 100–300 m wide and up to 500 m thick, located on the southern edge of the hydrothermal area, interpreted as altered, demagnetized basalt in a hydrothermal pipe. The pipe diameter is comparable to that of other modeled hydrothermal pipes at active hydrothermal sites on the MAR (site TAG, 200 m) [Tivey *et al.*, 1993], the Juan de Fuca Ridge (80 m on various sites on the Endeavour segment [Tivey and Johnson, 2002]), and the Kerma-dec Arc (Brothers volcano, ~ 200 –800 m) [Caratori-Tontini *et al.*, 2012b]. The 200 m southwestward shift of the pipe with respect to the hydrothermal area may either reflect the initial geometry of an eccentric or inclined pipe, as suggested in other areas [Caratori-Tontini *et al.*, 2012b], or result from the mass wasting effect of the observed landslides [Cannat *et al.*, 2013].

Our forward models show that a ~ 100 m thick hydrothermal deposit overlying the magnetized basement and a ~ 300 m wide eccentric pipe of nonmagnetic altered basalt can account for the magnetic anomalies observed at Krasnov. The maximum volume of the hydrothermal deposit is about 2.7×10^7 m³, as the nonmagnetic deposit may also contain magnetically incoherent basaltic debris flows. The volume of the nonmagnetic altered basalt is of the order of 3.5×10^7 m³. The base of the altered zone, marked by the lowest RTP magnetic anomaly, is located at equal horizontal distance, about 300 m, from both the major faults of the area (Figure 2). If the hydrothermal circulation, and therefore the altered zone, was controlled by the intersection of these faults, they should be dipping $\sim 30^\circ$, as shown by simple geometrical considerations. Although we have no constraint on the geometry of these faults at depth, their exposed section [see Cannat *et al.* 2013, Figure 5b] is compatible with such a 30° dip. These considerations support the inference that the Krasnov hydrothermal site formed as the result of focused hydrothermal circulation at the intersection of the two major faults.

5. Conclusion

Krasnov, an inactive basalt-hosted hydrothermal site, exhibits a strong negative magnetic anomaly, as all the active basalt-hosted hydrothermal sites investigated to date. This magnetic signature over an inactive site shows that, among the three processes proposed to account for the missing magnetization at basalt-hosted hydrothermal sites, the dominant ones are (1) the presence of thick hydrothermal deposits which increase the distance between the magnetic measurements and the underlying magnetic basalt, resulting in an apparent magnetic low and (2) the alteration of the strongly magnetic titanomagnetite of the underlying basalt to less magnetic titanomaghemite and ultimately to nonmagnetic minerals [e.g., Irving, 1970; Johnson and Atwater, 1977] as a result of the pervasive hydrothermal circulation beneath the site. Thermal demagnetization of the extrusive basalt has only a marginal contribution, if any, to this magnetic signature during hydrothermal activity.

Reaching a thickness of a hundred meters or more at major hydrothermal sites, the nonmagnetic hydrothermal deposits should be taken into account to investigate and model the near-seafloor magnetic signature of hydrothermal sites. The occurrence, on all basalt-hosted hydrothermal sites magnetically investigated so far, of zones of permanently altered rocks underlines the importance of the hydrothermal discharges in the geochemical fluxes of the oceans.

While the active hydrothermal sites are usually found with the help of their chemical and physical plumes in the water column, there is no such simple way to detect inactive sites. The latter are, however, much better targets for seafloor mineral exploration—they do not host fragile hydrothermal ecosystems and are not affected by high thermal gradients. A major consequence of our findings at Krasnov is that the presence of hydrothermal sulfides and the permanent destruction of magnetic minerals create a magnetic signature in basalt-hosted hydrothermal sites that can be used to detect and characterize both active and inactive hydrothermal sites. Near-seafloor magnetic surveys using ROVs or AUVs (autonomous underwater vehicle) can therefore be an important component of any deep-sea mineral exploration program.

Acknowledgments

We thank the captain and crew of R/V *Pourquoi pas?* and the technical team of ROV *Victor* for excellent work at sea during cruise *Serpentine*. This research was supported by CNRS, Ifremer, and IGP through several grants and fellowships. Chie Honsho deserves our gratitude for offering the opportunity to use her ABIC inversion method to perform the reduction to the pole. Discussions with Maurice Tivey, Fabio Caratori-Tontini, and Fabrice Fontaine are acknowledged. Careful reviews by Udo Barckhausen and an anonymous reviewer helped to improve the manuscript. This is IGP contribution 3521.

References

- Ade-Hall, J. M., H. C. Palmer, and T. P. Hubbard (1971), The magnetic and opaque petrological response of basalt to regional hydrothermal alteration, *Geophys. J. R. Astron. Soc.*, *24*, 137–174.
- Baranov, V. (1957), A new method for interpretation of aeromagnetic maps: Pseudo-gravimetric anomalies, *Geophysics*, *22*, 359–383.
- Bel'tenev, V., A. Shagin, V. Markov, I. Rozhdestvenskaya, T. Stepanova, G. Cherkashev, I. Fedorov, A. Rummyantsev, and I. Poroshina (2004), A new hydrothermal field at 16°38.4'N, 46°28.5'W on the Mid-Atlantic Ridge, *InterRidge News*, *13*, 5–6.
- Cande, S. C., and D. V. Kent (1995), Revised calibration of the geomagnetic polarity timescale for the late Cretaceous and Cenozoic, *J. Geophys. Res.*, *100*, 6093–6095.
- Cannat, M., A. Mangeney, H. Ondréas, Y. Fouquet, and A. Normand (2013), High-resolution bathymetry reveals contrasting landslide activity shaping the walls of the Mid-Atlantic Ridge axial valley, *Geochem. Geophys. Geosyst.*, *14*, 996–1011, doi:10.1002/ggge.20056.
- Caratori-Tontini, F., B. Davy, C. De Ronde, R.W. Embley, M. Leybourne, and M. A. Tivey (2012a), Crustal magnetization of Brothers Volcano, New Zealand, measured by autonomous underwater vehicles: Geophysical expression of a submarine hydrothermal system, *Econ. Geol.*, *107*, 1571–1581.
- Caratori-Tontini, F., C. De Ronde, D. Yoerger, J. Kinsey, and M. Tivey (2012b), 3-D focused inversion of near-seafloor magnetic data with application to the Brothers volcano hydrothermal system, Southern Pacific Ocean, New Zealand, *J. Geophys. Res.*, *117*, B10102, doi:10.1029/2012JB009349.
- Cherkashov, G., V. Bel'tenev, V. Ivanov, L. Lazareva, M. Samovarov, V. Shilov, T. Stepanova, G. P. Glasby, and V. Kuznetsov (2008), Two new hydrothermal fields at the Mid-Atlantic Ridge, *Mar. Georesour. Geotechnol.*, *26*(4), 308–316.
- Dyment, J., K. Tamaki, H. Horen, Y. Fouquet, K. Nakase, M. Yamamoto, M. Ravilly, and M. Kitazawa (2005), A positive magnetic anomaly at Rainbow hydrothermal site in ultramafic environment, *Eos Trans. AGU*, *86*(52), Fall Meet. Suppl., Abstract OS21C-08.
- Fouquet, Y., et al. (2008), *Serpentine cruise - ultramafic hosted hydrothermal deposits on the Mid-Atlantic Ridge: First submersible studies on Ashadze 1 and 2, Logatchev 2 and Krasnov vent fields*, *InterRidge News*, *18*, 15–19.
- Gee, J., S. Webb, J. Ridgway, H. Staudigel, and M. Zumberge (2001) A deep-tow magnetic survey of Middle Valley, Juan de Fuca Ridge, *Geochem. Geophys. Geosyst.*, *2*, 1059, doi:10.1029/2001GC000170.
- Honsho, C., J. Dyment, K. Tamaki, M. Ravilly, H. Horen, and P. Gente (2009), Magnetic structure of a slow spreading ridge segment: Insight from near-bottom magnetic measurements onboard a submersible, *J. Geophys. Res.*, *114*, B05101, doi:10.1029/2008JB005915.
- Honsho, C., T. Ura, and K. Kim (2013), Deep-sea magnetic vector anomalies over the Hakurei hydrothermal field and the Bayonnaise knoll caldera, Izu-Ogasawara arc, Japan, *J. Geophys. Res.*, *118*, 5147–5164, doi:10.1002/jgrb.50382.
- Honsho, C., T. Ura, and K. Tamaki (2012), The inversion of deep-sea magnetic anomalies using Akaike's Bayesian information criterion, *J. Geophys. Res.*, *117*, doi:10.1029/2011JB008611.
- Humphris, S. E., et al. (1995), The internal structure of an active sea-floor massive sulphide deposit, *Nature*, *377*, 713–716.
- IAGA (International Association of Geomagnetism and Aeronomy) Working Group V-MOD (2010), International Geomagnetic Reference Field: The eleventh generation, *Geophys. J. Int.*, *183*, 1216–1230, doi:10.1111/j.1365-246X.2010.04804.x.
- Irving, E. (1970), The mid-Atlantic ridge at 45°N, XIV, oxidation and magnetic properties of basalts: Review and discussion, *Can. J. Earth Sci.*, *7*, 1528–1538.
- Isezaki, N. (1986), A new shipboard three-component magnetometer, *Geophysics*, *51*(10), 1992–1998.
- Johnson, H. P., and T. Atwater (1977), Magnetic study of basalts from the Mid-Atlantic Ridge, lat, 37°N, *Geol. Soc. Am. Bull.*, *88*, 637–647.
- Johnson, H. P., and J. E. Pariso (1987), The effects of hydrothermal alteration on the magnetic properties of oceanic crust: Results from drill holes CY-2 and CY-2a, Cyprus Crustal Study Project, in *Cyprus Crustal Study Project: Initial Report, Holes CY2 and 2a*, edited by P. T. Robinson et al., pp. 283–293, *Geol. Surv. Can. Pap.* 85-29.
- Johnson, H. P., et al. (2002), Survey studies hydrothermal circulation on the northern Juan de Fuca Ridge, *Eos Trans. AGU*, *83*, 73–79.
- Kent, D. V., and J. Gee (1996), Magnetic alteration of zero-age oceanic basalt, *Geology*, *24*, 703–706.
- Nakamura, K., T. Toki, N. Mochizuki, M. Asada, J. Ishibashi, Y. Nogi, S. Yoshikawa, J. Miyazaki, and K. Okino (2013), Discovery of a new hydrothermal vent based on an underwater, high-resolution geophysical survey, *Deep Sea Res., Part 1*, *74*, 1–10.
- Smith, W. H. F., and P. Wessel (1990) Gridding with continuous curvature splines in tension, *Geophysics*, *55*, 293–305, doi:10.1190/1.1442837.
- Tivey, M. A. (1994), High-resolution magnetic surveys over the Middle Valley mounds, northern Juan de Fuca Ridge, *Proc. Ocean Drill. Program Sci. Results*, *139*, 29–35.
- Tivey, M. A., and J. Dyment (2010), The magnetic signature of hydrothermal systems in slow-spreading environments, in *Diversity of Hydrothermal Systems on Slow Spreading Ocean Ridges*, *AGU Monogr. Ser.*, vol. 188, edited by P. A. Rona et al., pp. 43–66, AGU, Washington, D. C., doi:10.1029/2008GM000773.
- Tivey, M. A., and H. P. Johnson (2002), Crustal magnetization reveals subsurface structure of Juan de Fuca Ridge hydrothermal vent fields, *Geology*, *30*(11), 979–982.
- Tivey, M. A., P. A. Rona, and H. Schouten (1993), Reduced crustal magnetization beneath the active sulfide mound, TAG hydrothermal field, Mid-Atlantic Ridge at 26°N, *Earth Planet. Sci. Lett.*, *115*, 101–116.
- Tivey, M. A., P. A. Rona, and M. C. Kleinrock (1996), Reduced crustal magnetization beneath relict hydrothermal mounds: TAG hydrothermal field, Mid-Atlantic Ridge, 26°N, *Geophys. Res. Lett.*, *23*(23), 3511–3514, doi:10.1029/96GL02082.
- Watkins, N. D., and T. P. Paster (1971), The magnetic properties of igneous rocks from the ocean floor, *Philos. Trans. R. Soc. London A*, *268*, 507–550.
- Zhu, J., J. Lin, Y. J. Chen, C. Tao, C. R. German, D. R. Yoerger, and M. A. Tivey (2010), A reduced crustal magnetization zone near the first observed active hydrothermal vent field on the Southwest Indian Ridge, *Geophys. Res. Lett.*, *37*, L18303, doi:10.1029/2010GL043542.